This article was downloaded by: [Siauliu University Library]
On: 17 February 2013, At: 06:58
Publisher: Taylor & Francis
Informa Ltd Registered in England and Wales Registered Number: 1072954 Registered office: Mortimer House, 37-41 Mortimer Street, London W1T 3JH, UK


Advanced Composite Materials
Publication details, including instructions for authors and subscription information:
http://www.tandfonline.com/loi/tacm20

# Damage propagation in CFRP laminates subjected to low velocity impact and static indentation

Yuichiro Aoki [a], Hiroshi Suemasu [b] & Takashi Ishikawa [c]

[a] Advanced Composite Evaluation Technology Center, Japan Aerospace Exploration Agency, 6-13-1 Ohsawa, Mitaka-shi, Tokyo 181-0015, Japan

[b] Department of Mechanical Engineering, Sophia University, 7-1 Kioi-cho, Chiyoda-ku, Tokyo 105-8554, Japan

[c] Advanced Composite Evaluation Technology Center, Japan Aerospace Exploration Agency, 6-13-1 Ohsawa, Mitaka-shi, Tokyo 181-0015, Japan

Version of record first published: 02 Apr 2012.

To cite this article: Yuichiro Aoki , Hiroshi Suemasu & Takashi Ishikawa (2007): Damage propagation in CFRP laminates subjected to low velocity impact and static indentation, Advanced Composite Materials, 16:1, 45-61

To link to this article: http://dx.doi.org/10.1163/156855107779755318

PLEASE SCROLL DOWN FOR ARTICLE

Full terms and conditions of use: http://www.tandfonline.com/page/terms-and-conditions

This article may be used for research, teaching, and private study purposes. Any substantial or systematic reproduction, redistribution, reselling, loan, sub-licensing, systematic supply, or distribution in any form to anyone is expressly forbidden.

The publisher does not give any warranty express or implied or make any representation that the contents will be complete or accurate or up to date. The accuracy of any instructions, formulae, and drug doses should be independently verified with primary sources. The publisher shall not be liable for any loss, actions, claims, proceedings, demand, or costs or damages whatsoever or howsoever caused arising directly or indirectly in connection with or arising out of the use of this material.

*Adv. Composite Mater.*, Vol. 16, No. 1, pp. 45–61 (2007)
© VSP 2007.
Also available online - www.brill.nl/acm

Downloaded by [Siauliu University Library] at 06:58 17 February 2013

# Damage propagation in CFRP laminates subjected to low velocity impact and static indentation

YUICHIRO AOKI [1,*], HIROSHI SUEMASU [2] and TAKASHI ISHIKAWA [1]

[1] *Advanced Composite Evaluation Technology Center, Japan Aerospace Exploration Agency, 6-13-1 Ohsawa, Mitaka-shi, Tokyo 181-0015, Japan*
[2] *Department of Mechanical Engineering, Sophia University, 7-1 Kioi-cho, Chiyoda-ku, Tokyo 105-8554, Japan*

Received 21 September 2005; accepted 6 March 2006

**Abstract**—This paper describes a damage accumulation mechanism in cross-ply CFRP laminates $[0_2/90_2]_{2S}$ subjected to out-of-plane loading. Drop-weight impact and static indentation tests were carried out, and induced damage was observed by ultrasonic C-scan and an optical microscope. Both tests gave essentially the same results for damage modes, sizes, and load-deformation history. First, a crack occurred in the bottom 0° layer accompanying some delamination along the crack caused by bending stress. Then, transverse cracks occurred in the middle 90° layer with decreasing contact force between the specimen and the indenter. Measured local strains near the impact point showed that the stress state changed from a bending dominant state to an in-plane tensile dominant state. A cohesive interface element was used to simulate the propagation of multiple delaminations and transverse cracks under static indentation. Two types of analytical models are considered, one with multiple delaminations and the other with both multiple delaminations and transverse cracks. The damage obtained for the model with only multiple delaminations was quite different from that obtained from the experiment. However, the results obtained from the model with both delaminations and transverse cracks well explain the characteristics of the damage obtained in the experiment. The existence of the transverse cracks is essential to form the characteristic impact damage.

*Keywords*: Delamination; transverse crack; low velocity impact; indentation; finite element analysis; cohesive element; progressive failure analysis.

## 1. INTRODUCTION

In recent years, the use of composite structures has increased, allowing the achievement of weight reductions owing to their high specific strength and stiffness. However, structures made of composite laminates are susceptible to low-velocity impact damage because no reinforcement exists through the thickness and there are

*To whom correspondence should be addressed. E-mail: aoki.yuichiro@jaxa.jp

material discontinuities at the ply interfaces. Delaminations at the ply interfaces and transverse cracks along the fibers are the characteristic damage features of laminated structures. This damage, being difficult to detect from the outside, causes severe reductions in the compressive performance of the structures. This phenomenon is commonly known as the CAI (Compression After Impact) problem [1–5]. Design loads of composite structures are often limited by their degraded compressive strength. Therefore, it is important to understand the mechanism of damage accumulation in composite laminates subjected to low-velocity impact.

The low-velocity impact test is sometimes replaced by static indentation tests since the damage configuration due to static indentation is similar to that of low-velocity impact [6–10]. The impact damage in composite laminates consists of delaminations, transverse cracks, and fiber breakages. The accumulation process of this damage is quite complex, and hence it is reasonable to investigate the damage problem under static loading instead of the complex impact response, and thereby avoiding such dynamic effects.

Analytical tools that can simulate damage growth are required to clarify the damage accumulation problems in composite laminates. Along with the increase of computer performance, finite element analysis has become a powerful tool for simulating the behavior of damage and failure procedures. Various numerical methods have been proposed to study the mechanism of damage accumulation in composite laminates. The virtual crack closure technique (VCCT) has been successfully used to study the stability of delamination propagation under the assumptions of initial delaminated area and self-similar delamination growth [11, 12]. In order to simulate progressive delaminations, interface models based on damage mechanics have been proposed and developed [13–17]. Delamination propagation is taken into account by means of material degradation, which depends on the internal damage variable. On the other hand, a cohesive crack model based on the Dugdale-Barenblatt cohesive zone approach [18, 19] has also been introduced, but it is only applicable when the cohesive zone size is small when compared with the size of the crack and specimen.

The mechanical response of the cohesive model is determined by traction and energy dissipation in the vicinity of a crack tip. The so-called cohesive zone model is convenient and attractive for simulating the delamination propagation in composite laminates since the fracture interface can be prescribed. Various cohesive elements have been developed and proposed for simulating the crack-like damage in composite materials [20–29].

In this paper, damage growth in cross-ply CFRP laminates is studied experimentally and numerically. Drop–weight impact and static indentation tests are performed for the purpose of comparing the results. The load history and laminate responses are measured to consider the damage initiation and growth. A numerical model using a three-dimensional cohesive element is used to simulate the growth of multiple delaminations and transverse cracks in cross-ply laminates subjected to

Downloaded by [Siauliu University Library] at 06:58 17 February 2013

static indentation. The coupling effect between the transverse cracks and delaminations on the laminate behavior and final damage shape are discussed.

## 2. EXPERIMENTAL

### *2.1. Preparation of specimens*

This study used T800/3633 carbon fiber/epoxy laminate manufactured by Toray Industries, Inc., because this material system had a large amount of available basic material data on the JAXA-ACDB web site [30]. The stacking sequence of the specimen is $[0_2/90_2]_{2S}$ with a nominal fiber volume fraction of 58% and an average thickness of 2.26 mm. The specimen selected here is based on one of the CAI test methods, the so-called Half-SACMA (H-SACMA) [31], which has been proposed as more economical than the conventional SACMA method [32] in terms of specimen size. Specimens of 76 mm width and 102 mm length were cut out of a mother plate. In order to examine the responses of the laminates during impact or static tests, uniaxial strain gages (Kyowa, KFG-2-120-C1-11L1M2R) were glued to the top and bottom surfaces of the specimen. The strain gage was 2 mm length, 120 ohm resistance and gage factor of 2.11. The dimensions of the H-SACMA specimen and the gage locations are shown in Fig. 1.

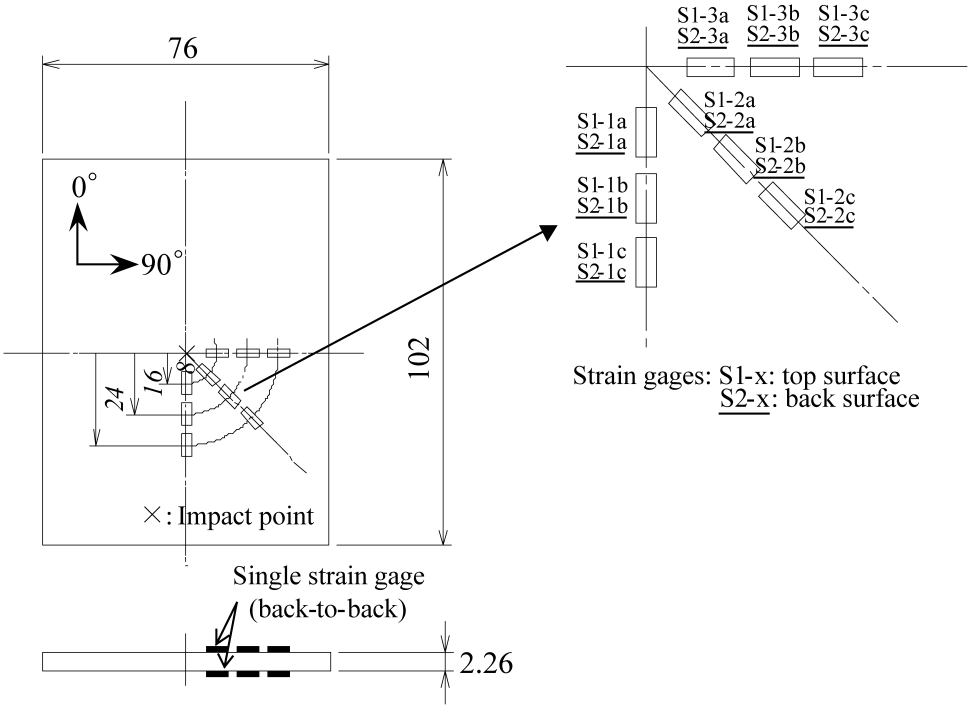


**Figure 1.** Schematic view of H-SACMA specimens and locations of strain gages.

Downloaded by [Siauliu University Library] at 06:58 17 February 2013

Downloaded by [Siauliu University Library] at 06:58 17 February 2013

### *2.2. Impact and static indentation tests*

Impact was given to the center of the specimens with an Instron 9250HV drop–weight impact test machine with a 15.9 mm (5/8 inch) hemispherical steel tip. The total mass of the impactor was 5.07 kg. Impact energies from 5.02 J to 15.07 J were obtained by changing the drop height, from which impact velocities ranged from 1.42 m/s to 2.42 m/s.

The support fixture consisted of a support base with a cut-out of 80 mm × 60 mm and a picture frame type support holder with the same size cut-out. Specimens were placed on the support base, and the holder was clamped to the base by fasteners tightened by hand. The contact force history of the specimen was obtained by the instrumented tip. Strains were measured by a high-speed data acquisition device (Yokogawa WE7000) with a sampling rate of 100 kHz during an impact event.

Static indentation tests were carried out by the Instron 4400R screw driven testing machine. Specimens were tested at a constant displacement rate of 0.5 mm/min. The same indenter and support fixture as those used in the impact tests were used in the static tests. In the static tests, the load was applied up to the maximum contact force level measured in the impact tests. The total energies given by the indenter were 0.89 J, 1.55 J, 4.54 J and 5.97 J, which were calculated from the area under the load–deflection curve of the specimen. In order to investigate the damage initiation and propagation in detail, the energy smaller than impact test was applied to the specimen in indentation test. Figure 2 shows a specimen placed inside the support fixture.

After the tests, the sizes and shapes of areas of damage were inspected by the ultrasonic C-scan system (Krautkramer SDS 5400R) for all specimens. The specimens were scanned immersed in water in pulsed-echo mode by a 5.0 MHz transducer. Some of the static indentation tests were stopped at various load levels, and the specimens were cut into slices by a diamond fine saw. The sliced specimens

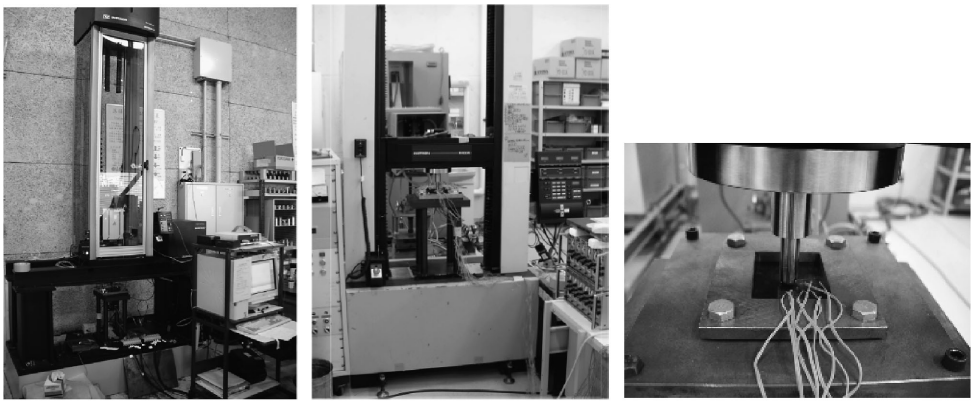

(a) Impact test machine (b) Static indentation test machine (c) Support fixture

**Figure 2.** Overview of support fixtures.

were then mounted in epoxy resin and ground by abrasive papers to observe the initial damage and damage growth by the optical microscope.

### *2.3. Test results and discussion*

Typical C-scan images of specimens after the impact and static indentation tests are shown in Fig. 3. Each specimen was subjected to 5.02 J and 4.54 J, respectively. It was found that the aspects of the damage were quite similar, while the damage size of the impact test was slightly larger than that of the static test. The relationship between contact force and displacement is shown in Fig. 4. The contact force for the static and impact tests increased with displacement until it dropped suddenly at 1.8 kN with unstable damage growth. The load subsequently increased nonlinearly in both tests due to the large deflection. After the sudden force drop, the deflection in the impact test was larger than that of the static test, and the unloading responses

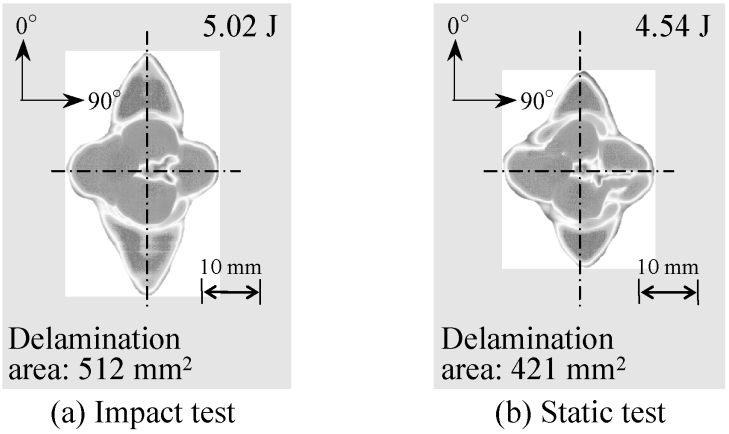


**Figure 3.** Typical damage due to impact and static tests.

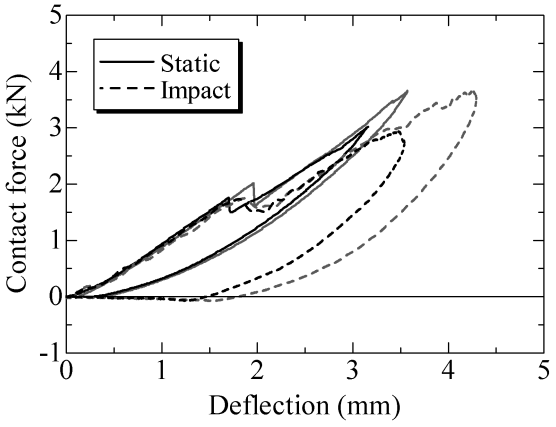


**Figure 4.** Typical loadforce–deflection curves.

Downloaded by [Siauliu University Library] at 06:58 17 February 2013

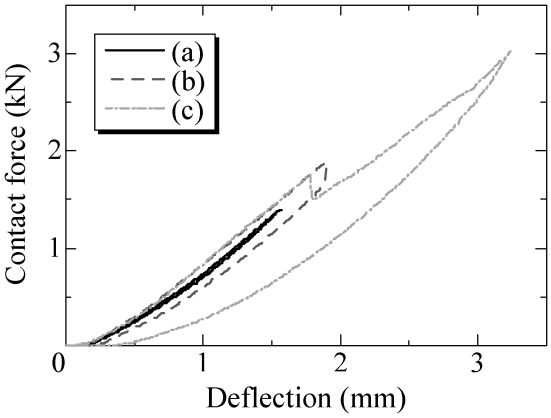


**Figure 5.** Load–deflection curves for different energy levels: (a) First cracking noise perceived (0.89 J), (b) Sudden load–drop occurred with sharp noise (1.55 J), (c) Damage propagated significantly (5.97 J).

showed a crucial difference between the two cases. In the impact test the deflection was not measured but calculated from the integral of the impact velocity measured by the instrumented velocity detector, and this might cause considerable error in the traveling distance of the impactor.

Figure 5 shows load–deflection curves for static indentation tests. Three specimens were loaded up to three different load levels corresponding to: the first cracking noise perceived by the ear (1.4 kN, 0.89 J), a sudden load–drop that occurred with a sharp noise (1.9 kN, 1.55 J), and after the propagation of considerable damage (3.0 kN, 5.79 J). Figure 6 shows ultrasonic C-scan images of the damage in which the depth information from the top surface is indicated. Figure 7 shows the micrographs of the cross-section under the indented position for the specimen loaded at the each load level.

From the micrographs, the first instance of damage occurred without a visible load-drop when a single bending crack in the bottom layer and transverse cracks in the second bottom layer (90° layer) were observed. This damage caused a little delamination in the lowest 90°/0° interface along the bending crack, shown in Fig. 6(a). The load-drop was caused by the unstable growth of the damage, i.e. the combination of the transverse cracks inclined at 45° in the middle 90° layer and the delaminations. The transverse cracks created inverse pine tree shape damage, which was found in the impact loading [33]. The number of transverse cracks then increased, and the delaminations propagated in the same shape with the load increase. In the present study, delaminations in the lowest 90°/0° interface and the second 0°/90° interface were larger than other delaminations, and there were more transverse cracks in the backside layers than in the topside layers.

Figure 8(a) shows the load and typical strain histories during the impact test. Strains were obtained from the back-to-back strain gages shown in Fig. 1. Strain at gage S2-1a was broken due to the bending crack propagation. A load-drop at 2.2 ms

Downloaded by [Siauliu University Library] at 06:58 17 February 2013

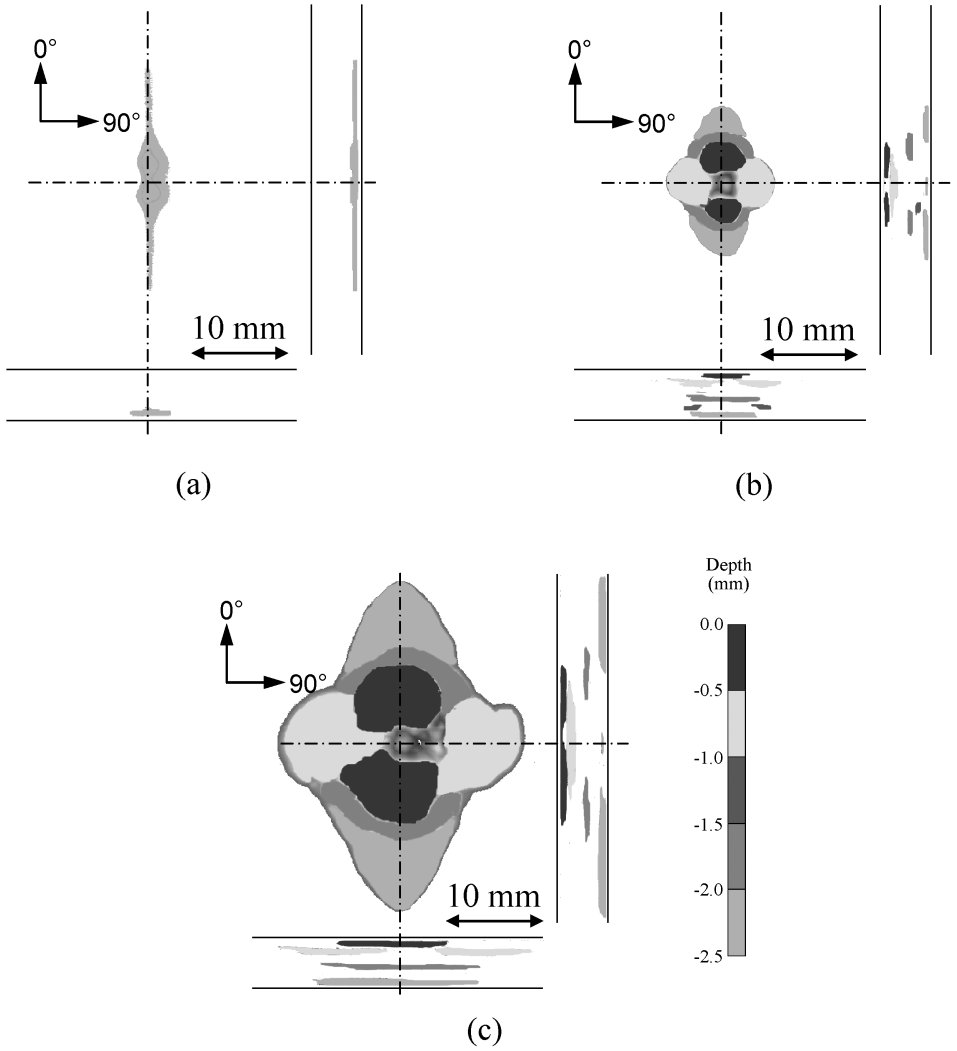


**Figure 6.** Ultrasonic images for different load levels due to static indentation. The upper figure of each image is the plane view (C-Scope) and the lower and side figures are the cross-section view (B-Scope). (a) At first noise (0.89 J), (b) After sudden load–drop (1.55 J), (c) After damage propagated significantly (5.97 J).

caused a reduction of the strain S1-3b, where the transverse cracks appeared in the middle 90° layer and the associated delamination propagated. It is shown from the back-to-back strains of S1-1b and S2-1b that bending of the laminate was dominant at a low load level, but the compressive strain at gage S1-1b changed to tensile strain with load increases. The effect of the in-plane stiffness due to large deflection became pronounced compared to the bending stiffness with the increase of load. Therefore, the laminate was in tensile condition even in the top surface. Bending and in-plane stresses induced large tensile strains on the backside of the laminates,

Downloaded by [Siauliu University Library] at 06:58 17 February 2013

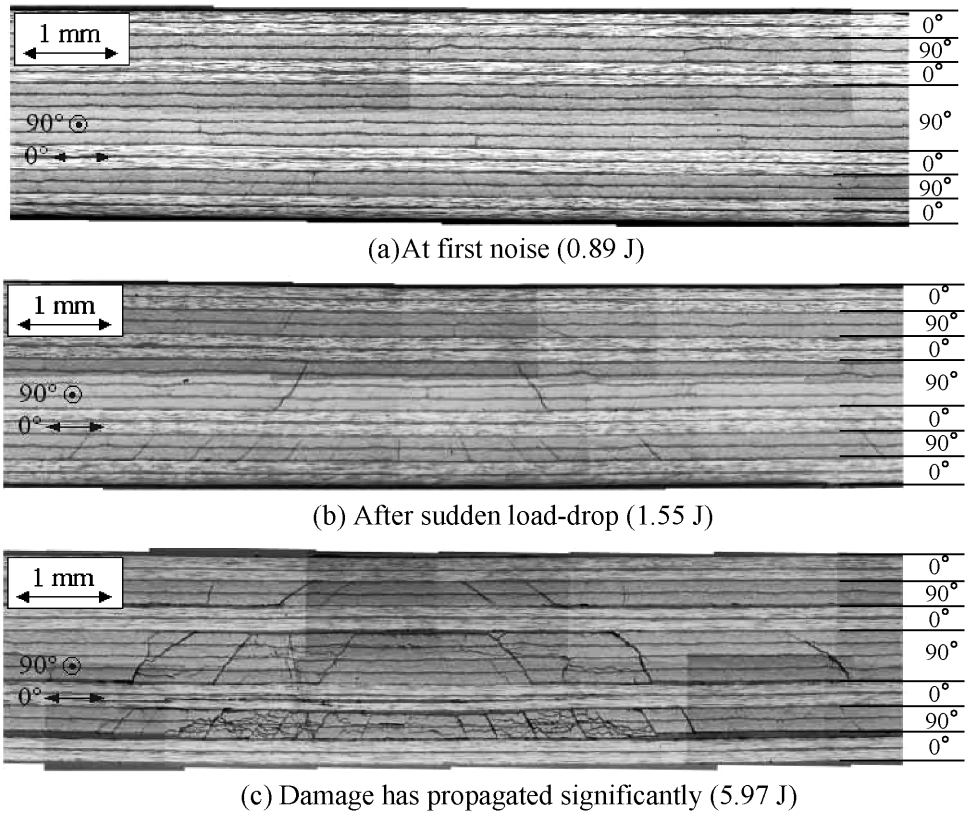


**Figure 7.** Micrographs of the cross-section for different load levels due to static indentation.

and hence there were many cracks in the backside layers. At the maximum load, the strain data showed drastic changes due to delamination propagation under the strain gages. Similar behavior and the same strain levels were shown in the case of the static indentation test as well, as shown in Fig. 8(b). This indicates that the dynamic effect could be a secondary factor in damage evolution.

Both tests gave essentially the same results regarding the damage size and shape of the laminates. Therefore, it can be concluded that the static indentation test can be an effective and reasonable test method to approximately study the low-velocity impact phenomenon of composite structures, thus avoiding the difficulty of the data measurement during impact load.

## 3. FINITE ELEMENT ANALYSIS

### *3.1. Formulation of the cohesive interface element*

In order to study the damage growth mechanism in cross-ply laminates, numerical analysis using a three-dimensional cohesive element was conducted. The concept

Downloaded by [Siauliu University Library] at 06:58 17 February 2013

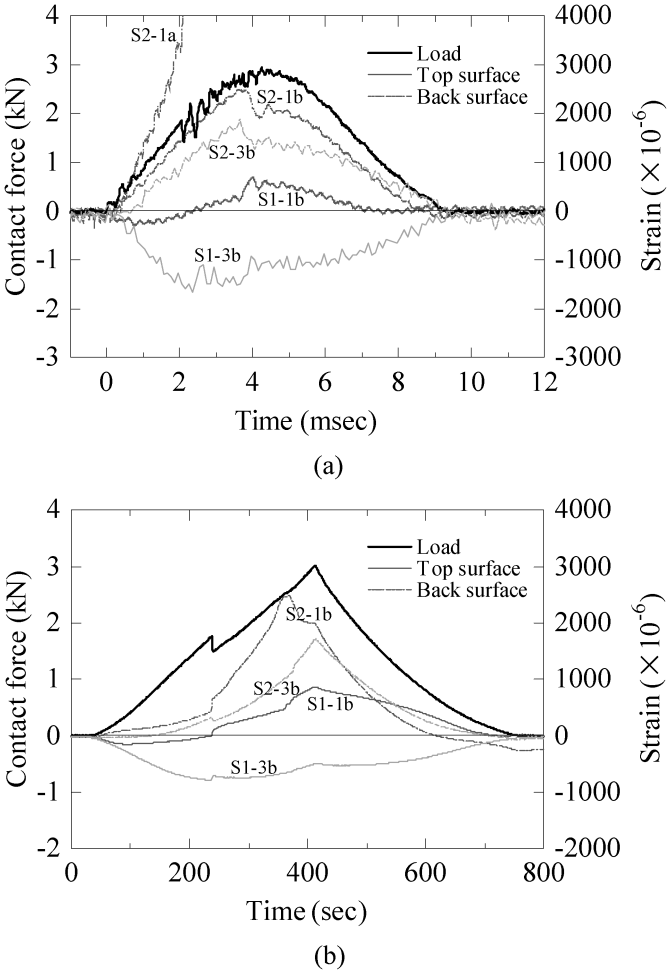


**Figure 8.** Load and typical strain histories during impact and static tests: (a) impact test, (b) static test.

of the cohesive element is shown in Fig. 9. The $x$–$y$–$z$ and $\xi$–$\eta$ are global and local coordinate systems, respectively. The cohesive element used here consists of 16 nodes and its thickness is nearly zero ($10^{-6}$ mm). The cohesive element is introduced into the interface between ordinary 20-node solid elements to model delaminations and transverse cracks. Such damage can propagate only along the element boundaries. The stiffness of the cohesive elements is reduced to zero when the interface deforms over the designated value. The constitutive relation of the cohesive element is derived by a specific separation energy density which is a function of relative displacements. The relative movement of the element is divided into two modes, the opening mode (Mode I) and sliding mode (Modes II and III). Without loading, node $i$ in the lower surface and node $i'$ in the upper surface have the same $x$–$y$ coordinates in the model. The relative sliding displacements $\Delta u$, $\Delta v$

Downloaded by [Siauliu University Library] at 06:58 17 February 2013

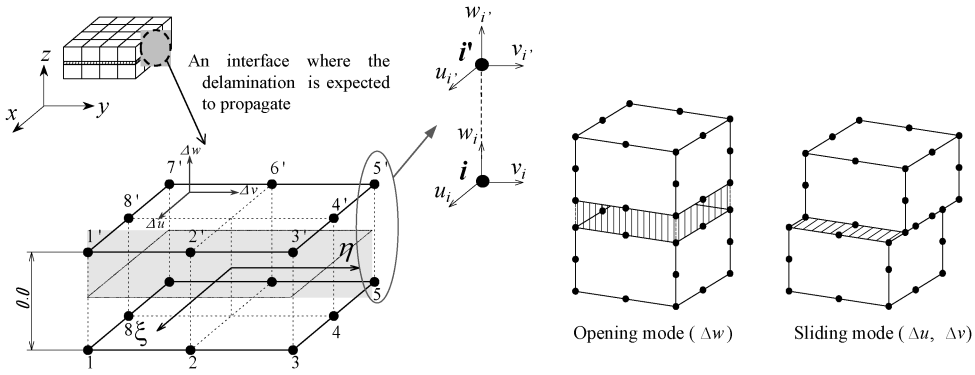


**Figure 9.** Geometry of the present cohesive element.

and opening displacement $\Delta w$ are defined as

$$\Delta u = \sum_{i=1}^{8} \phi_i(\xi, \eta)\Delta u_i, \quad \Delta v = \sum_{i=1}^{8} \phi_i(\xi, \eta)\Delta v_i, \quad \Delta w = \sum_{i=1}^{8} \phi_i(\xi, \eta)\Delta w_i,$$
$$\Delta u_i = u_{i'} - u_i, \quad \Delta v_i = v_{i'} - v_i, \quad \Delta w_i = w_{i'} - w_i, \tag{1}$$

where $\phi_i(\xi, \eta)$ is the shape function and $u_i$, $v_i$, $w_i$ and $u_{i'}$, $v_{i'}$, $w_{i'}$ are components of nodal displacement at nodes $i$ and $i'$, respectively. The separation energy density per unit area stored in the element is defined by a function of the relative displacements as follows:

$$\Phi = G_c\{1 - \exp(-\varphi)\} + f(\Delta w),$$
$$\varphi = \alpha\Delta w^2 + \beta(\Delta u^2 + \Delta v^2), \tag{2}$$

where

$$f(\Delta w) = \begin{cases} k_c \Delta w^2 & (\Delta w < 0) \\ 0 & (\Delta w \geqslant 0) \end{cases}$$

and where $G_c$ is a critical total energy release rate, and $\alpha$ and $\beta$ are coefficients that determine the critical tractions and critical relative displacements. The second term of the right-hand side $f(\Delta w)$ is a penalty function introduced to consider the contact problem at the failed surface. When the relative displacement $\Delta w$ is negative, the normal penalty stiffness $k_c$ is applied to prevent the interface from overlapping. The tractions in each direction at node $i$ are given in the following forms.

$$T_{ui} = \int\!\!\int_{A_e} \frac{\partial \Phi}{\partial \Delta u}\phi_i \, \mathrm{d}A_e, \quad T_{vi} = \int\!\!\int_{A_e} \frac{\partial \Phi}{\partial \Delta v}\phi_i \, \mathrm{d}A_e, \quad T_{wi} = \int\!\!\int_{A_e} \frac{\partial \Phi}{\partial \Delta w}\phi_i \, \mathrm{d}A_e, \tag{3}$$

where

$$\mathrm{d}A_e = |\mathbf{J}| \, \mathrm{d}\xi \, \mathrm{d}\eta, \quad \mathbf{J}\text{: Jacobian} \quad (i = 1\text{–}8).$$

Downloaded by [Siauliu University Library] at 06:58 17 February 2013

Tangent stiffness matrix $\mathbf{K}_{\mathrm{t}}$ of the element is derived by the derivative of the traction vector $\mathbf{T}$ with respect to the nodal displacements $\Delta\mathbf{u}$ as

$$\delta\mathbf{f}_i = \mathbf{K}_{\mathbf{t},ij}\delta\Delta\mathbf{u}_j = \frac{\partial\mathbf{f}_i}{\partial\Delta\mathbf{u}_j}\delta\Delta\mathbf{u}_j. \tag{4}$$

Figure 10 illustrates the energy density function and constitutive relations for opening and sliding modes. The tractions are plotted against the relative opening displacement $\Delta w$ and sliding displacement $\Delta u$ ($\Delta v$). The traction becomes a maximum value $T_{wc}$ (or $T_{uc}$, $T_{vc}$) at a critical relative displacement $\Delta w_{\mathrm{c}}$ (or $\Delta u_{\mathrm{c}}$, $\Delta v_{\mathrm{c}}$), and then decreases to zero at $\Delta w_0$ ($\Delta u_0$, $\Delta v_0$), at which point the energy density function reaches a critical energy release rate of $G_{\mathrm{c}}$. The shape of the traction-displacement curve and different weights to the sliding and normal opening displacement contributions are determined by the coefficients $\alpha$ and $\beta$. The maximum traction value can be set to the interfacial debonding strength. The element separates completely when damage parameter $D = \Phi/G_{\mathrm{c}}$ reaches a value of 1.0 and all the cohesive forces vanish. Once the element separates completely, the damage parameter is stored in the stiffness calculation in order to prevent the recovery of the interface in the unloading process. The component of tangent stiffness reduces to a very small value ($=10^{-20}$) after the damage parameter reaches

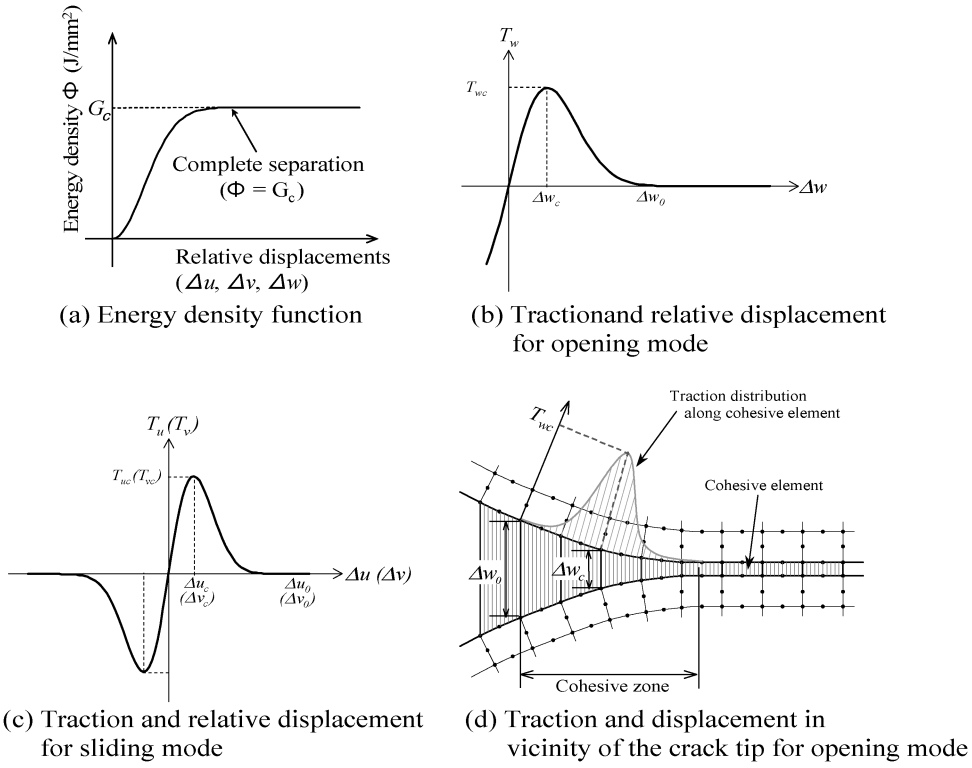


**Figure 10.** Relationship between energy density function and tractions.

Downloaded by [Siauliu University Library] at 06:58 17 February 2013

a value of 1.0. The cohesive zone near the crack tip is schematically illustrated in Fig. 10(d). Since the neighborhood of the crack tip area deforms significantly, the elements should be sufficiently small compared to the cohesive zone. The interface element is implemented in the finite element code ABAQUS 6.4 using the user subroutine UEL [34].

### *3.2. Analytical model*

The present cohesive element was applied to simulate the damage propagation in cross-ply laminates $[0_2/90_2]_{2S}$ under static indentation. Only a quarter of the model inside the support cut-out was analyzed, as shown in Fig. 11. Dimensions of the numerical model were 30 mm × 40 mm × 2.26 mm. In the present analysis, in order to reduce the computational cost, only the center region of 16 mm × 16 mm was modeled by three-dimensional 20-node solid element (C3D20) and 15-node solid element (C3D15), while the other region was modeled by three-dimensional 8-node composite shell element (S8R), where the shell and solid regions were connected by multi-point constraints (MPC) in the ABAQUS option [34]. The material properties used for the laminates and the cohesive elements are summarized in Tables 1 and 2. The critical energy release rate $G_c$ of 1.6 kJ/m$^2$ given to the cohesive elements was equal to the critical Mode II fracture toughness of the present material [30]. The maximum tractions in the sliding direction were equal to the interlaminar shear debonding strength. The value of $10^4$ N/mm is used for the penalty stiffness $k_c$ based on previous analyses. The boundary conditions were applied in accordance with the test conditions, and displacement–loading was applied to the center of the laminates.

Two types of analysis models, A and B, were considered in order to examine the effect of transverse cracks on delamination propagation. Model A has only

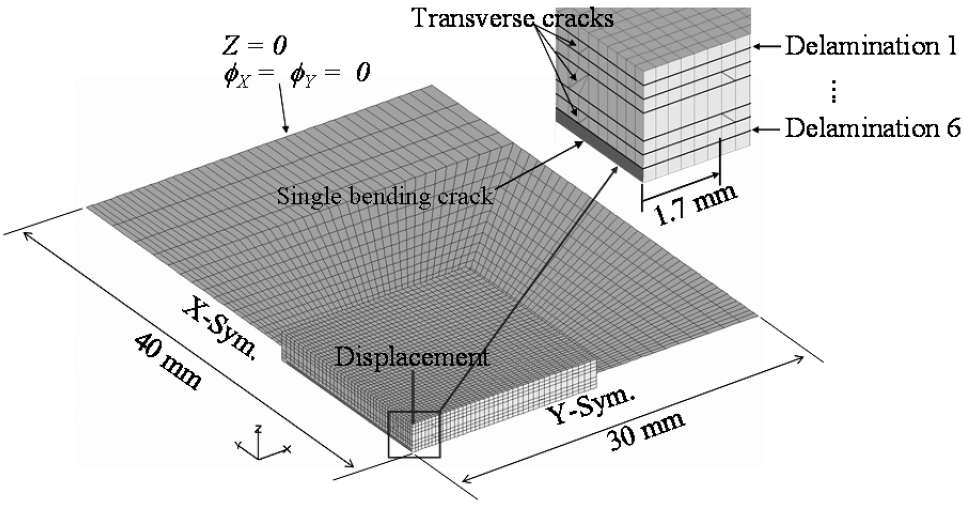


**Figure 11.** Typical finite element mesh of the cross-ply laminates with transverse cracks (Model B).

Downloaded by [Siauliu University Library] at 06:58 17 February 2013

**Table 1.**
Properties of the cross-ply laminates

| $E_{11}$* | $E_{22}$* $= E_{33}$ | $\upsilon_{12}$* $= \upsilon_{13}$ | $\upsilon_{23}$ | $G_{12} = G_{13}$ | $G_{23}$ |
|---|---|---|---|---|---|
| 156.3 GPa | 8.9 GPa | 0.34 | 0.45 | 5.6 GPa | 3.07 GPa |

* Referred to JAXA-ACDB [30].

**Table 2.**
Properties of the cohesive element

| $G_c$* | $T_{w_c}$ | $T_{u_c} = T_{v_c}$* | $\Delta w_c$ | $\Delta u_c = \Delta v_c$ |
|---|---|---|---|---|
| 1.6 kJ/m$^2$ | 20 MPa | 116 MPa | $5.0 \times 10^{-2}$ mm | $8.6 \times 10^{-3}$ mm |

* Referred to JAXA-ACDB [30].

Downloaded by [Siauliu University Library] at 06:58 17 February 2013

delaminations and Model B has not only delaminations but also transverse cracks at each lamina. In Model A, cohesive elements are introduced only to each interface to simulate delamination propagation. In Model B, the cohesive elements are used for the propagation of transverse cracks in each layer as well as for delaminations. As shown in Fig. 11, the geometry of the transverse cracks can be simplified based on microscopic observation of the cross-section (see Fig. 7), which is inclined at 45° in each layer (except for the top and bottom layers) and arranged to be parallel to the fiber direction of the layer. A single bending crack is modeled at its center in the bottom layer, and there is no transverse crack in the top layer. At each delaminated area, the edges of the transverse cracks exist below and above the delamination. The number of 20-node solid and 8-node shell elements is 27,466 while that of cohesive elements is 17,310 in Model A, and in Model B these numbers are 27,898 and 17,754, respectively. The fracture toughness of the transverse and bending cracks is equal to that of the delamination. The location of the delamination is indicated by the number that increases from top to bottom through the thickness. The geometrical nonlinearity due to finite deflection is also considered. The Newton-Raphson iterative approach was used for the nonlinear finite element analysis. In order to stabilize the convergence of the solution, solution control parameters were modified by the CONTROL option [34].

### *3.3. Analytical results*

Figure 12 shows the relationship between the reaction force of the indented position and deflection of the cross-ply laminates. Damage propagations under the indented position at different load levels are shown in Fig. 13. The first delamination propagation occurs at the center of the interlaminar plane (delaminations 2, 3 and 4) with some reduction of the stiffness in Model A, since transverse shear stress across the delamination is usually large at its middle surface. After the first delamination, the stiffness reduction becomes clear when all of the delaminations propagate stably in the same shape in the fiber direction of the layer below the

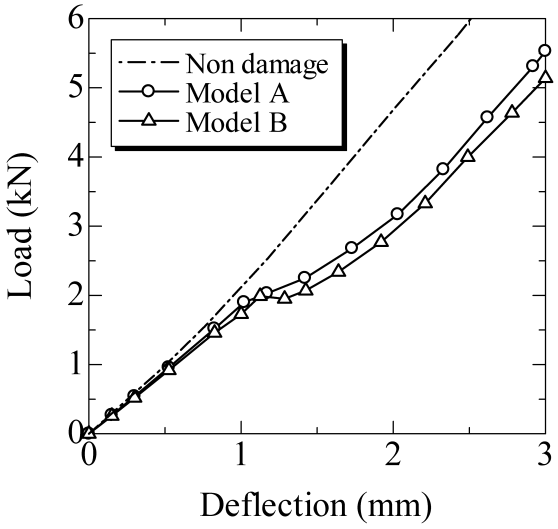


**Figure 12.** Relationship between the reaction force of the indented position and deflection of the cross-ply laminates.

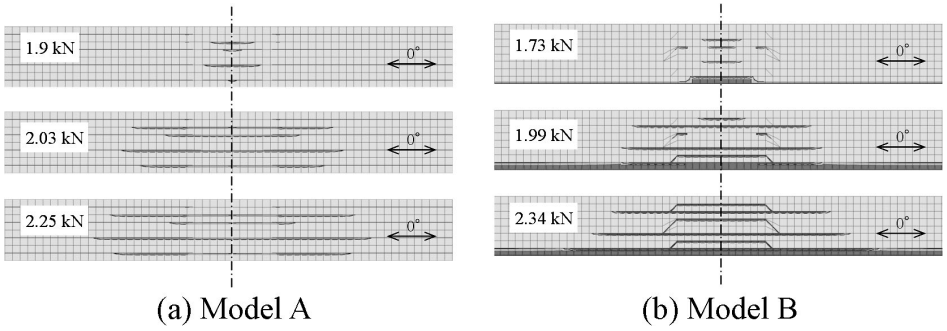


**Figure 13.** Comparison of predicted delamination shapes under indented position.

delaminations. In Model B, the first occurrences of damage were a bending crack and adjacent delamination 6 propagated along the crack tip at a load of 1.5 kN. Delaminations 2, 3 and 4 also propagated at the same load level. Then, delamination 5 and a transverse crack in the 90° layer propagated simultaneously at 2.0 kN, and the bending crack propagated completely. Following this, all of the transverse cracks and delaminations propagated unstably at the same increment where the load decreased slightly, and where the load increased nonlinearly the delamination propagated stably with the same shape. Delamination tends to be large at the middle layer in Model A and at the bottom in Model B. Further, the initial damage propagation in Model B is more complicated and unstable than in Model A because of the existence of transverse cracks.

A comparison of predicted delamination shapes at a load level of 2.3 kN as obtained by Models A and B are shown in Fig. 14, where damage parameter $\Phi/G_c$

Downloaded by [Siauliu University Library] at 06:58 17 February 2013

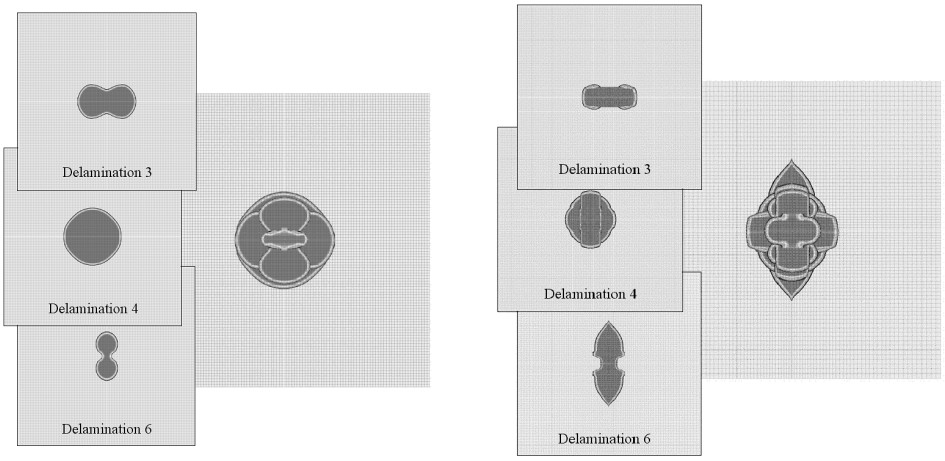


**Figure 14.** Comparison of predicted delamination shapes at 2.3 kN.

is plotted. The general tendency of delamination propagation is basically similar in both models. All the delaminations propagate in the fiber direction of the layer below their interfaces. The predicted delamination shape of Model B was sharper than that of Model A. The delamination shape in Model A was continuous and more circular as a whole. Delamination 4 was the largest while delamination 1 was the smallest through the thickness. On the other hand, the delamination shape in Model B was discontinuous at the edges of the transverse cracks below and above the delamination. The most interesting point here is that delamination 6, just near the bottom surface, became large in the fiber direction when compared to the other delaminations, which are elongated along the bending crack. Moreover, this tendency seems to be stronger with an increase of load. This result well explains the characteristics of real damage, i.e., impact damage, which has very large delamination near the bottom surface.

## 4. CONCLUSION

A damage growth problem in cross-ply CFRP laminates under low-velocity impact and static indentation was studied. Both tests gave essentially the same results for damage modes, delamination size, and deformations of the laminates. The different stages of the damage growth were observed by experiments and simulated by finite element analysis. Bending and in-plane stresses induced large tensile strains on the backside of the laminate, and hence there were many cracks in the backside layers. After the damage initiation, the laminate was in tensile condition even in the top surface, which caused extensive delamination propagation. A numerical model with a cohesive interface element was applied to the propagation of the

Downloaded by [Siauliu University Library] at 06:58 17 February 2013

delamination and transverse cracks in the laminate due to the static indentation. Two types of analytical models were considered in order to examine the effect of transverse cracks on delamination propagation. One model had only delaminations while the other had both delaminations and transverse cracks. The analytical results show that the general tendency of delamination propagation was basically similar in both cases. All of the delaminations propagated in the fiber direction of the layer below their interfaces. However, the stability of the initial delamination and each delamination shape were quite different. The final delamination shape was influenced by existing transverse cracks. The delamination adjacent to the bottom layer was elongated along the bending crack and sharp at the crack. The result obtained from the delaminations and transverse cracks model well explains the characteristics of realistic damage. The effect of transverse cracks on predicted delamination propagation is significant.

Downloaded by [Siauliu University Library] at 06:58 17 February 2013

## REFERENCES


1. S. Liu, F. K. Chang, S. Liu. and F. K. Chang, Matrix cracking effect on delamination growth in composite laminates induced by a spherical indenter, *J. Compos. Mater*. **28**, 940–977 (1994).
2. S. A. Hichen and R. M. J. Kemp, The effect of stacking sequence on impact damage in a carbon fiber/epoxy composite, *Composites* **26**, 207–214 (1995).
3. T.-W. Shyr and Y.-H. Pan, Impact resistance and damage characteristics of composite laminates, *Compos. Struct*. **62**, 193–203 (2003).
4. T. Ishikawa, S. Sugimoto, M. Matsushima and Y. Hayashi, Some experimental findings in CAI tests of CF/PEEK and conventional CF/EPOXY flat plates, *Compos. Sci. Technol*. **55**, 349–362 (1995).
5. E. F. Dost, L. B. Ilcewicz and W. B. Avery, The effects of stacking sequence on impact damage resistance and residual strength for quasi-isotropic laminates, *ASTM STP* **1110**, 476–500 (1991).
6. P. O. Sjöblom, J. T. Hartness and T. M. Cordell, On low-velocity impact testing of composite materials, *J. Compos. Mater*. **22**, 30–52 (1988).
7. E. Wu and K. Shyu, Response of composite laminates to contact loads and relationship to low-velocity impact, *J. Compos. Mater.* **27**, 1443–1464 (1993).
8. S. M. Lee and P. Zahuta, Instrumented impact and static indentation of composites, *J. Compos. Mater*. **25**, 204–222 (1991).
9. H. Kaczmarek and S. Maison, Comparative ultrasonic analysis of damage in CFRP under static indentation and low-velocity impact, *Compos. Sci. Technol*. **51**, 11–26 (1994).
10. F. Aymerich, P. Priolo and D. Vacca, Static loading and low-velocity impact characterization of graphite/PEEK laminates, *The e-Journal of Nondestructive Testing* **4**, 3 (1999).
11. H. Razi and A. S. Kobayashi, Delamination in cross-ply laminated composite subjected to low-velocity impact, *AIAA J*. **31**, 1498–1502 (1993).
12. S. Liu and F. K. Chang, Matrix cracking effect on delamination growth in composite laminates induced by a spherical indenter, *J. Compos. Mater*. **28**, 940–977 (1994).
13. O. Allix and P. Ladevèze, Damage analysis of interlaminar fracture specimens, *J. Compos. Mater.* **31**, 61–74 (1995).
14. V. Albouyso, O. Allix, P. Ladevèze and D. Leveque, Interfacial Approach of Delamination: Possibilities and Difficulties, in: *Proc. ICCM-12*, Paris, France, CD-Rom (1999).
15. Y. Mi, M. A. Crisfield, G. A. O. Davies and H. B. Hellweg, Progressive delamination using interface elements, *J. Compos. Mater*. **32**, 1246–1273 (1998).

16. C. Alfano and M. A. Crisfield, Finite element interface models for the delamination analysis of laminated composites: mechanical and computational issues, *Int. J. Numer. Meth. Engng.* **50**, 1701–1736 (2001).
17. W. Sprenger, F. Gruttmann and W. Wagner, Delamination growth analysis in laminated structures with continuum-based 3D-shell elements and a viscoplastic softening model, *Comput. Meth. Appl. Mech. Engng*. **185**, 123–139 (2000).
18. D. S. Dudgale, Yielding of steel sheets containing slits, *J. Mech. Phys. Solids*, **8**, 100–104 (1960).
19. G. I. Barenblatt, Mathematical theory of equilibrium cracks in brittle failure, *Adv. Appl. Mech*. **7**, 55–129 (1962).
20. A. Hillerborg, M. Modeer and P. E. Petersson, Analysis of crack formation and crack growth in concrete by means of fracture mechanics and finite elements, *Cement and Concrete Research* **6**, 773–782 (1976).
21. A. Needleman, A continuum model for void nucleation by inclusion debonding, *J. Appl. Mech*. **54**, 525–531 (1987).
22. A. Needleman, An analysis of decohesion along an imperfect interface, *Int. J. Fracture* **42**, 21–40 (1990).
23. S. El-Sayed and S. Sridharan, Predicting and tracking interlaminar crack growth in composites using a cohesive layer model, *Composites Part B* **32**, 545–553 (2001).
24. G. Lin, P. H. Geubelle and N. R. Sottos, Simulation of fiber debonding with friction in a model composite pushout test, *Int. J. Solids Struct*. **38**, 8547–8562 (2001).
25. R. Borg, L. Nilsson and K. Simonsson, Modeling of delamination using a discredited cohesive zone and damage formulation, *Compos. Sci. Technol*. **62**, 1299–1314 (2002).
26. C. G. Davila, Mixed mode decohesion elements for analyses of progressive delamination, in: *Proc. 42nd AIAA/ASME/ASCE/AHS/ASC Structures, Structural Dynamics, and Materials Conf.*, Seattle, AIAA paper 2001-1486 (2001).
27. V. K. Goyal, E. R. Johnson, C. G. Davila and N. Jaunky, An irreversible constitutive law for modeling the delamination process using interface elements, in: *Proc. 43rd AIAA/ASME/ASCE/AHS/ASC Structures, Structural Dynamics, and Materials Conf.*, Denver, CO, AIAA paper 2002-1576 (2002).
28. A. Cornec, I. Scheider and K. H. Schwalbe, On the practical application of the cohesive model, *Engng. Fracture Mech*. **70**, 1963–1987 (2003).
29. Y. Aoki and H. Suemasu, Damage analysis in composite laminates by using interface element, *Adv. Compos. Mater.* **12**, 13–22 (2003).
30. Advanced Composites Database System, JAXA-ACDB; Ver.04-1, *http://www.jaxa-acdb.com/*
31. T. Ishikawa and M. Matsushima, in: *Proc. of the 9th US–Japan Confer. Compos. Mater.*, Shizuoka, pp. 133–140 (2000).
32. SACMA Recommended Method SRM 2R-94, Suppliers of Advanced Composite Materials Association, Arlington, VA (1994).
33. S. Abrate, *Impact on Composite Structures*. Cambridge University Press (1998).
34. ABAQUS Ver.6.4 Analysis User's Manual Vol. I-IX, ABAQUS, Inc. (2003).

Downloaded by [Siauliu University Library] at 06:58 17 February 2013